A Comparative Study on Conformation and Ligand Binding of the Neuronal Uncoupling Proteins

ARTICLE *in* BIOCHEMISTRY · DECEMBER 2009

Impact Factor: 3.02 · DOI: 10.1021/bi901742g

6 AUTHORS, INCLUDING:

Tuan Hoang
McGill University
18 PUBLICATIONS **119** CITATIONS
SEE PROFILE

Matthew D. Smith
Wilfrid Laurier University
45 PUBLICATIONS **1,166** CITATIONS
SEE PROFILE

Masoud Jelokhani-Niaraki
Wilfrid Laurier University
44 PUBLICATIONS **546** CITATIONS
SEE PROFILE

512 *Biochemistry* **2010,** *49,* 512–521
DOI: 10.1021/bi901742g

BIOCHEMISTRY
including biophysical chemistry & molecular biology
Article

A Comparative Study on Conformation and Ligand Binding of the Neuronal Uncoupling Proteins[†]

Marina V. Ivanova,[‡] Tuan Hoang,[‡] Fern R. McSorley,[‡,§] Gabriela Krnac,[‡,§]
Matthew D. Smith,[§] and Masoud Jelokhani-Niaraki*[,‡]

[‡]*Departments of Chemistry and* [§]*Biology, Wilfrid Laurier University, Waterloo, Ontario N2L 3C5, Canada*

Received October 8, 2009; Revised Manuscript Received November 23, 2009

ABSTRACT: Mitochondrial uncoupling proteins of the nervous system (UCPs 2, 4, and 5) have potential roles in the function and protection of the central nervous system (CNS). In the absence of structural information, conformations of the hexahistidine-tagged versions of all five human UCPs in liposomes were investigated for the first time, using far- and near-UV CD and fluorescence spectroscopy. Highly pure UCPs 1−5 were reconstituted in detergents and stable small unilamellar vesicles, appropriate for spectroscopic studies. All UCPs formed dominantly helical conformations in negatively charged phospholipid vesicles (palmitoyloleoylphosphatidylcholine/palmitoyloleoylphosphatidylglycerol, 7:3 molar ratio). UCPs 2 and 5 exhibited comparable helical conformations with possible association in lipid bilayers, whereas UCP4 had a different helical profile that can be related to its less associated form. Interaction of reconstituted UCPs with GDP and GTP, inhibitors of the prototypic UCP1, was detected by near-UV CD and fluorescence spectroscopy, utilizing the sensitivity of these techniques to microenvironments around Trp residues close to the nucleotide binding site. Binding of UCP4 to purine nucleotides was also different from other UCPs. Binding of fatty acids, activators of proton transport in UCPs, to UCPs could not be unambiguously detected, implying a nonbinding conformation/orientation of the proteoliposomes. Interaction of CoA with UCPs was comparable to nucleotide binding, suggesting a possible binding of this molecule at the nucleotide binding site. Despite dissimilar primary sequences, neuronal UCPs share common structural and functional properties with UCPs 1 and 3, supporting a common physiological role in addition to their specific roles in the CNS.

Uncoupling proteins (UCPs), located in the inner mitochondrial membrane, uncouple ATP synthesis from the respiratory chain by transporting protons into the matrix, hence dissipating the protonmotive force. In BAT, this physiological function is mediated by the uncoupling protein, UCP1, also known as thermogenin. In addition to thermogenesis, several other functions have been suggested for the proton leak pathways including regulation of energy metabolism, control of body mass, and attenuation of ROS production (*1*). The UCPs are members of the anion-carrier protein family located in the inner mitochondrial membrane, and a total of five mammalian UCPs are known to date (*2*). UCP3 and neuronal UCPs (nUCPs),[1] which include UCPs 2, 4, and 5, were discovered in the late 1990s (*2*−*5*). UCP3 has been mostly found in skeletal muscle and heart tissues (*1*, *2*). UCP2 has been found in several mammalian tissues, and its expression in the CNS is primarily in the hypothalamus, limbic system, cerebellum, choroid plexus, brainstem, neurons, and glial cells (*2*, *6*). UCP4 was initially found to be exclusively expressed in the brain; recently, however, this protein was also discovered in adipocytes (*4*, *7*). UCP5 has been found in various tissues including brain, testis, uterus, kidneys, lung, stomach, liver, and heart (*1*, *5*, *6*). A comparison between the primary sequences of all five human UCPs (hUCPs) is exhibited in Figure 1. The number of amino acids in hUCPs 1−5, their relative size, and the composition of their basic/acidic and aromatic amino acid residues are shown in Table 1.

Mitochondrial nUCPs have numerous potential roles in support of the function and survival of CNS, including thermal synapses, enhanced synaptic neurotransmission, calcium regulation, mitochondrial proliferation and biogenesis, reduction of ROS production, pain and ethanol tolerance/sensitivity, synapse regulation, and synaptic plasticity (*6*, *8*). Furthermore, the aforementioned UCP-induced mitochondrial effects can be relevant to numerous neurodegenerative diseases, such as epilepsy, Parkinson's disease, ischemia/stroke and traumatic brain injury, Alzheimer's disease, amyotrophic lateral sclerosis, and aging (*6*, *8*, *9*).

The activation of UCP1, the most studied UCP, is presumed to be mediated by fatty acids (*1*, *2*). So far, two plausible mechanisms have been proposed for UCP1 proton transport: the proton-buffering model and the fatty acid-cycling model (*2*). It has been shown that Asp^{28} in UCP1 (conserved in all UCPs 1−3 and

[†]The present study was supported by grants from the Canada Foundation for Innovation and the Natural Sciences and Engineering Research Council of Canada to M.J.-N. (CFI, 6786; NSERC, 250119) and M.D.S. (CFI, 11292; NSERC, 312143). M.V.I. was the recipient of an Ontario Graduate Scholarship. T.H. has been a recipient of NSERC undergraduate USRA and graduate CGSM scholarships.

*To whom correspondence should be addressed. Tel: (519) 884-1970 (ext 2284). Fax: (519) 746-0677. E-mail: mjelokhani@wlu.ca.

[1]Abbreviations: ANT1, ADP/ATP translocase 1; ATCC, American Type Culture Collection; BAT, brown adipose tissue; CD, circular dichroism; CNS, central nervous system; CoA, coenzyme A; DDM, *n*-dodecyl β-D-maltoside; EB, extraction buffer; FTIR, Fourier-transform infrared; IB, inclusion body; IMAC, immobilized metal affinity chromatography; LA, lauric acid (sodium salt); NRMSD, normalized root mean square deviation; POPC, 1-palmitoyl-2-oleoyl-*sn*-glycero-3-phosphocholine; POPG, 1-palmitoyl-2-oleoyl-*sn*-glycero-3-phospho-(1′-*sn*-glycerol) (sodium salt); ROS, reactive oxygen species; SUV, small unilamellar vesicle; TEV, tobacco etch virus; TM, transmembrane; (n)UCP, (neuronal) uncoupling protein.

 Published on Web 12/14/2009

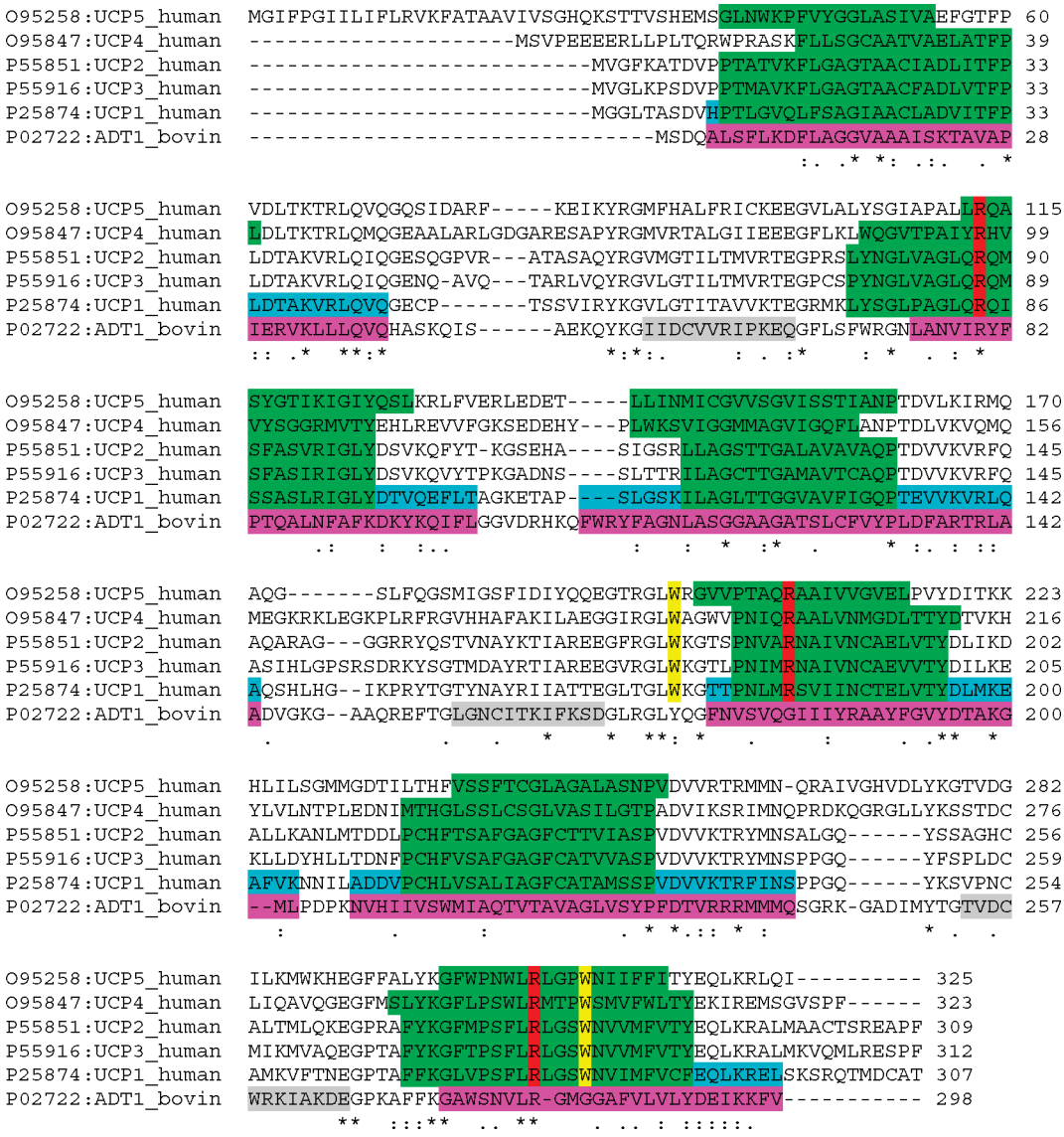

FIGURE 1: Sequence alignment of human UCPs. Alignment of the amino acid sequence of hUCPs 1−5 and bovine ANT1, based on the EBI Clustal W2 Multiple Sequence Alignment Tool and Swiss-Prot entries hUCP1 (P25874), hUCP2 (P558519), hUCP3 (P55916), hUCP4 (O95847), hUCP5 (O95258), and ANT1 (P02722) (*34*). The identical residues are denoted by an asterisk, the conserved substitutions by a colon, and the semiconserved substitutions by a decimal point. Methionine, the initiator amino acid for protein biosynthesis, is included in all sequences. Conserved Arg residues (red) involved in nucleotide binding and conserved Trp residues (yellow) are shown in vertical boxes. For UCPs, TM domains 1−6, based on hydrophobicity scales, are shown in horizontal green boxes; sequences of the six TM (magenta) and three matrix (light gray) helical domains of ANT1 are based on the crystal structure of this protein in complex with carboxyatractyloside (*22*); extended TM domains for UCP1, aligned with the helical TM domains of ANT1, are highlighted in light blue.

Table 1: Comparison of Human UCP Primary Sequences[a]

hUCP	no. of AA	MW (kDa)	no. of acidic residues	no. of basic residues	overall charge	no. of Trp residues	no. of Tyr residues	no. of Phe residues
1	307	33.005	20	30	+10	2	8	13
2	309	33.229	19	34	+15	2	11	15
3	312	34.216	22	33	+11	2	12	15
4	323	36.064	31	37	+6	8	10	11
5	325	36.202	22	34	+12	6	10	19

[a]The length, molecular mass, and net charge of each hUCP and the number of their basic and acidic residues as well as the aromatic amino acid composition are shown. Data were obtained through the use of the ExPASy Proteomics Server and the Proteomic tool ProtParam, using accession numbers hUCP1 (P25874), hUCP2 (P55851), hUCP3 (P55916), hUCP4 (O95847), and hUCP5 (O95258). Methionine, the initiator amino acid in protein biosynthesis, is included in the number of AA counts. AA = amino acids; MW = molecular mass.

replaced with Glu in UCPs 4 and 5, Figure 1) plays an important role in proton transport, and when mutated to Asn, proton transport is drastically reduced but retained on replacement with Glu (*10*). Purine nucleotides bind tightly to UCP1 and are considered as both inhibitors and regulators of UCP1 activity. It has been proposed that the purine nucleotide binding site in

hUCP1, as determined by site-directed mutagenesis, involves three basic arginine residues (located in transmembrane domains TM2, TM4, and TM6) conserved in all five UCPs (Figure 1) (*1*, *11*). The proton conductance of UCP1 is under tight control: it is greatly enhanced by free fatty acids and strongly inhibited by purine nucleoside di- and triphosphates; however, these mechanisms are not yet fully understood (*1*, *2*). In addition to protons, UCP1 has been shown to transport anions (such as Cl^-, Br^-, and NO_3^-). Anion transport is also inhibited by nucleotides; however, fatty acids are not required for its activation (*12*).

It is noteworthy to mention that the typical UCP1-like biochemical and physiological properties of nUCPs 4 and 5 have not yet been clearly demonstrated; consequently, the question as to whether UCP4 and UCP5 are genuine mitochondrial UCPs remains to be proven (*1*). Furthermore, sequence alignment and analysis of transmembrane domains suggest that UCPs 1−3 on one hand and UCPs 4 and 5 on the other hand belong to separate subfamilies (*13*). It was speculated that UCP4 might represent the ancestral UCP from which the other invertebrate, mammalian, and plant UCPs diverged. Phylogenetically, it seems that UCPs 1−3 possibly arose later during evolution and hence are likely to fulfill more specialized functions (*14*).

UCPs share ~20% sequence identity with bovine ANT (ATP/ADP carrier; ANT1) membrane protein. It has been suggested that the structure of UCPs could be comparable to that of the ANT protein (*11*). All five UCPs and the ANT protein share a common tripartite structure that consists of three repeat domains each with two hydrophobic α-helical TM subdomains spanning the mitochondrial inner membrane (*1*). The two helices within each repeat are connected by a long loop that is oriented on the matrix side of the membrane.

To gain further insight into the potential importance of UCPs in neurodegenerative diseases, understanding the similarities and differences in their structure−function relationship is crucial. This comparative study is focused on the structure and ligand binding of the nUCPs, especially the less studied UCPs 4 and 5. All five human UCPs were expressed in *Escherichia coli*, isolated, and obtained in high purity. Subsequent reconstitution of the proteins in mild detergents or liposomes allowed for a detailed conformational analysis of nUCPs, involving interaction with known UCP activators and inhibitors, using CD and fluorescence spectroscopy.

EXPERIMENTAL PROCEDURES

Chemicals. Phospholipids POPC and POPG were from Avanti Polar. Detergents *N*-lauroylsarcosine (sodium salt) and digitonin were from Calbiochem-EMD Biosciences; DDM was from Sigma. Platinum Pfx DNA polymerase (Invitrogen) and Proofstart DNA polymerase (Qiagen) were used for all PCR amplifications. The TOPO cloning kit and all designed primers were from Invitrogen. His-Bind Ni-charged resin and the pET21 cloning vectors were from Novagen. The EZNA gel extraction kit was from Omega Bio-Tek, and the QIAprep spin miniprep kit was from Qiagen. T4 DNA ligase and all restriction enzymes were from New England Biolabs. Amberlite XAD-4 polymeric adsorbent beads were from Supelco. All other chemicals were of high-purity grade and used as received.

UCP Constructs. The hUCP2 cDNA clone (pET-hUCP2) was a gift from Dr. Martin Brand (MRC Dunn Human Nutrition Unit, Cambridge, U.K.). The hUCP1, hUCP3, and hUCP5 cDNA clones were purchased from ATCC, and each was received in a pCR-BluntII-TOPO vector. The hUCP4 cDNA was synthesized by Genscript Corp. and received as a pUC57 vector. The hUCP3 clone was subcloned into pET21a, and the other four hUCP clones were subcloned into pET21d. All clones included their endogenous stop codons. Primer adapters were used to incorporate 5′ *Nde*I (for hUCP3), 5′ *Nco*I (for hUCPs 1, 2, 4, and 5) and 3′ *Sal*I (for all five hUCPs) restriction sites into the ends of the hUCP cDNAs by PCR, which facilitated cloning into pET21 vectors, as well as the 5′ coding sequence for a hexahistidine tag and a TEV (tobacco etch virus) protease recognition site. The final five constructs, pET21a-TEV-hUCP3$_{His}$ and pET21d-TEV-hUCP1$_{His}$/-hUCP2$_{His}$/-hUCP4$_{His}$/-hUCP5$_{His}$, encode recombinant versions of the hUCPs that include an N-terminal His_6 tag separated from the endogenous start codon by a TEV protease recognition site (ENLYFQG). Subsequent cleavage of the His tag by the TEV protease would result in the full UCP protein with one additional glycine residue at the N-terminus. His tag removal was not attempted in this study, as it has been observed that the presence of the His tag does not affect the overall conformation or binding function of the proteins (*11*). The pET21d-TEV-hUCP1$_{His}$, pET21d-TEV-hUCP2$_{His}$, pET21a-TEVhUCP3$_{His}$, and pET21d-TEV-hUCP5$_{His}$ constructs were introduced into *E. coli* BL21(DE3), whereas the pET21d-TEV-hUCP4$_{His}$ construct was introduced into *E. coli* BL21CodonPlus (DE3)-RIPL to facilitate overexpression of the recombinant proteins.

Recombinant UCP Expression and Purification. Overexpression of all five recombinant hUCPs was achieved by induction with 1 mM IPTG (isopropyl β-D-thiogalactoside) for 3 h at 37 °C with aeration, as described previously (*11*). Cell pellets containing the recombinant protein were resuspended in EB (extraction buffer) [20 mM Tris-HCl (pH 8.0), 500 mM NaCl, and 20 mM imidazole], incubated for 20 min with lysozyme (200 μg/mL), and sonicated using a probe-tip sonicator. The IBs (inclusion bodies) were then collected by centrifugation at 86876*g* for 15 min at 4 °C using a TLA-100.3 rotor (Beckman Coulter) and washed four times using EB with 1% (w/v) Triton X-100 and once with EB. The final pellet was resuspended in EB containing 8 M urea and 1 mM THP [tris(hydroxypropyl)phosphine] and incubated for 4 h while sonicating with a probe-tip sonicator every 1 h. The protein suspension was then centrifuged [86876*g* for 15 min at 4 °C using a TLA-100.3 rotor (Beckman Coulter)] to remove all insoluble aggregates, and the supernatant was diluted with EB to a final urea concentration of 6 M. Proteins were then purified using Ni-NTA (Ni^{2+}-nitrilotriacetate) chromatography under denaturing conditions according to the manufacturer's protocol (Novagen). In brief, urea-solubilized inclusion bodies were applied to a Ni-resin preformed column. The resin was washed with EB containing 6 M urea and 40 mM imidazole, and the protein was eluted using EB containing 6 M urea and 500 mM imidazole.

Protein Determination and SDS−PAGE Analysis. Protein concentrations were determined using the DC RC Lowry protein assay kit (Bio-Rad Laboratories) suitable for detergent-containing samples. Proteins were separated and analyzed using SDS−PAGE gels containing a 4% stacking gel and a 12% resolving gel, stained with Coomassie Brilliant Blue R-250.

Preparation of Proteins in Detergent for CD Experiments. Purified hUCPs were precipitated using TCA (trichloroacetic acid) and washed twice with 0.5% (v/v) TCA and once with sterile water. The precipitated protein was resuspended in 250−450 μL (depending on apparent protein

content) of buffer A [10 mM potassium phosphate (pH 7.5)] with 2% (w/v) sarcosyl, sonicated in a bath sonicator, and incubated for 1 h at room temperature. The solubilized protein was diluted 4-fold with buffer A and then 5-fold with buffer B [0.2% (w/v) digitonin or 0.3% (w/v) DDM and 10 mM potassium phosphate (pH 7.5)] followed by an addition of 2% (w/v) sarcosyl to yield a final sarcosyl concentration of 0.16%, following the protocol by Jelokhani-Niaraki et al.(*11*). Buffer exchange and protein concentration were achieved via centrifugal diafiltration. Specifically, the solution was concentrated 3-fold by centrifugation at 5000*g* for 7 min at 4 °C (JA 30.50 Ti rotor; Beckman) in a centrifugal filter device with a 10 kDa molecular mass limit (Amicon Ultra 10K; Millipore), then diluted 3-fold with buffer B, and concentrated 3-fold again. This was repeated twice more using buffer B and then twice using buffer A. To remove any remaining sarcosyl, 2 mL of the protein solution was incubated overnight with Dowex mesh 16-50 (500 mg of the Cl^- form and 15 mg of the OH^- form for a 1.5 mg/mL protein concentration; Dow Chemical Co.) on a rotating mixer at 4 °C. The protein-containing solution was removed from the ion-exchange beads and was diluted before spectroscopic analysis to appropriate protein concentrations in a buffer composition of 0.02% (w/v) digitonin or 0.03% (w/v) DDM and 10 mM potassium phosphate (pH 7.5). In some instances, 10 mM Tris buffer (pH 7.5) was used instead of potassium phosphate buffer throughout the sample preparation procedure.

Preparation of SUVs and Reconstitution of Proteins for CD Experiments. The phospholipid vesicle system was composed of POPC/POPG (7:3 molar ratio) phospholipids to mimic a simple negatively charged membrane representing the inner membrane of mitochondria. The reconstitution method was based on a protocol by Echtay et al. (*15*). Briefly, a chloroform solution of 25 mg/mL lipid in the required ratio was dried under a mild nitrogen flow in a round-bottomed flask to form a thin layer. The film was dried overnight under vacuum and then rehydrated with buffer A. The resulting multilamellar vesicles were then sonicated on an ice bath using a probe-tip sonicator until a clear, transparent solution was obtained. The lipid dispersion was then centrifuged at 19500*g* for 15 min at room temperature (220.87 V05/6 rotor; Hermle) to remove any titanium particles, and the supernatant yielded unilamellar vesicles with an approximate diameter of 30−50 nm. The liposomes were allowed to equilibrate for 15 min before 20% (w/v) Triton X-100 was slowly added to obtain a final Triton X-100 concentration of 0.2%, and this solution was allowed to equilibrate for 1 h at room temperature.

Starting from the protein in 2% sarcosyl, the solution was diluted to 0.5% sarcosyl using buffer A. The liposome/Triton X-100 mixture was then added to the protein to obtain a final lipid/protein ratio of 100 and a Triton X-100/lipid ratio of 3. The mixture was allowed to equilibrate for 1 h at room temperature. The detergent was removed by shaking the protein−liposome−detergent mixture with Amberlite XAD-4 (Supelco) adsorbent resin (500 mg of beads/14 mg of detergent) overnight at 4 °C on a rotary shaker. The proteoliposome dispersion was then removed from the adsorbent beads and used for CD or fluorescence spectroscopic analysis.

CD Measurements and Analysis. CD spectra were measured on an Aviv 215 spectropolarimeter (Aviv Biomedical). Ellipticities are reported as mean residue ellipticity. The measurements were carried out in rectangular quartz cells with 0.1 cm (far-UV) and 0.5 cm (near-UV) path lengths. The spectra were measured at 0.2 or 0.5 nm/s (far-UV) and 0.5 nm/s (near-UV) scanning speed and reported as an average of four scans. CD spectra were analyzed further for estimation of secondary structure content by the deconvolution program CDSSTR, which uses a single value deconvolution algorithm (*16*, *17*). The analysis was based on a set of 48 reference proteins and performed on the Dichroweb Web site (*18*, *19*).

Fluorescence Measurements. All steady-state measurements were done with a Cary Eclipse fluorescence spectrophotometer (Varian). Intrinsic tryptophan and tyrosine fluorescence emission was measured at excitation wavelengths of 280 and 295 nm, with an excitation slit width of 5 nm and a scan speed of 600 nm/min. Proteoliposome samples in buffer A, with a protein/lipid molar ratio of ~0.01, were taken directly from CD measurement experiments. Measurements were performed at room temperature (~25 °C). Emission spectra were corrected by subtraction of the corresponding blank spectrum (including ligands, if applicable) of the liposome dispersion. Absorption of samples for fluorescence measurements was generally low, and therefore the correction for the inner filter effect was not applied.

RESULTS AND DISCUSSION

Expression and Purification of hUCPs. UCPs have previously been overexpressed as either IBs or recombinant His-tagged proteins in yeast and bacteria (*11*). In the current study, the His-tagged recombinant proteins hUCPs 1−5 were expressed in *E. coli* and had calculated molecular masses of 34.9, 35.1, 36.1, 37.9, and 38.1 kDa, respectively. Successful expression of the hUCP proteins was verified with dominant bands of the Triton X-100 washed IBs. The urea-solubilized protein was then purified using IMAC, and the successful purification was confirmed using SDS−PAGE (Figure 2). The degree of purification and protein yield were estimated from the eluted fractions to be ~85% or higher.

Conformation of Neuronal hUCPs in Detergents. Previous conformational studies on UCPs have been limited to FTIR and CD spectroscopy on UCP1 (*11*, *20*, *21*). FTIR studies showed that UCP1 from hamster, reconstituted in lipid−detergent micelles, was composed of approximately 50% α-helical, 30% β-sheet (mainly antiparallel), and 15% turn structure (*21*). Since a crystal structure of bovine mitochondrial ANT in complex with carboxyatractyloside was solved, it has been used as the structural basis for other mitochondrial carriers (*22*). The first documented CD study of UCPs concluded that His-tagged UCP1, in 0.03% DDM, consists of 68% α-helix (*20*). In a more recent CD study, in 0.02% digitonin, a 40−50% helical content was estimated for the mouse UCP1; in addition, in the same study it was shown that the first and second matrix loop domains of UCP1 can also contain elements of helical structure, hence contributing to the overall helical content of the protein (*11*). On the basis of hydrophobic scales, in UCP1, 122 amino acids are part of the TM domains and can potentially adopt helical conformations; consequently, a helical content of at least 40% can be assumed for this protein (Figure 1). In the ANT1 crystal structure, 67% of residues form helical structures, of which ~55% are from the TM domains and the remaining ~12% are due to the matrix loop domains (*22*). The TM segments of ANT1 are highlighted in Figure 1, and an alignment with the sequence of UCP1 is shown for comparison. Although the alignment of the TM domains of UCP sequences with that of ANT1 may show a more realistic picture of the TM sequences (and helical structure) in UCPs, in the absence of structural details, the overall tertiary

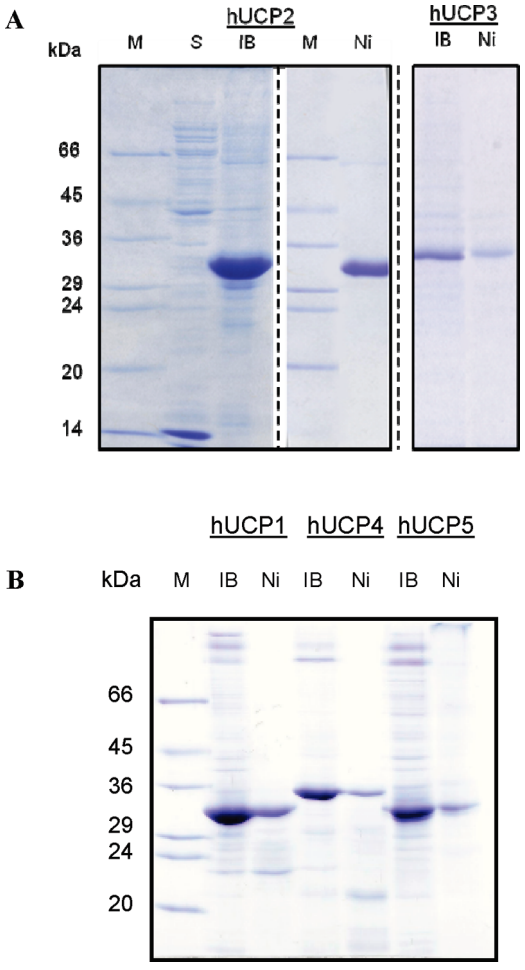

FIGURE 2: Expression and purification of recombinant human UCPs. Recombinant hUCPs were expressed in *E. coli*, extracted and purified by immobilized affinity chromatography (IMAC), resolved using SDS−PAGE (12% gel), and stained with Coomassie Brilliant Blue. (A) Soluble *E. coli* extract (S), Triton X-100 washed inclusion bodies (IB, 10 μg), and IMAC-purified protein (Ni, 5 μg) for hUCP2, and Triton X-100 washed inclusion bodies (IB, 5 μg) and IMAC-purified protein (Ni, 2 μg) for hUCP3. (B) Triton X-100 washed inclusion bodies (IB, 10 μg each) and IMAC-purified proteins (Ni, 5 μg each) for hUCP1, hUCP4, and hUCP5. Molecular mass markers (M) are indicated in kDa.

structure and the total content of secondary structure in UCPs remain speculative.

Members of the mitochondrial carrier family, such as ANT, and the phosphate carriers have been extensively studied and compared to UCPs. A proline signature sequence PX(D/E)XX-(K/R) conserved among all mitochondrial carriers (and all five UCPs) defines a hinge that may be involved in the translocation of substrates (*22*). Other similarities between UCP1 and ANT include partial structural identity, possibility of the existence of dimeric functional forms, and ability to bind nucleotides. Moreover, these two proteins are among the very few members of the mitochondrial anion carriers that do not possess a signal sequence for targeting to the mitochondria at the N-terminus of the protein (*23*).

CD spectra were measured for hUCPs in digitonin (data not shown; previously shown for UCP1 in ref *11*) and DDM, mild nonionic detergents used for the reconstitution of membrane proteins. The comparative far-UV CD spectra for hUCPs in DDM, normalized at 220 nm, are depicted in Figure 3. CD spectra of UCP1 and UCP3 are also included for comparison. The detergent con-

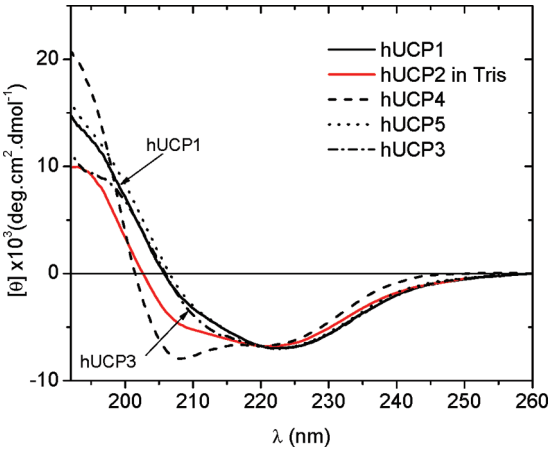

FIGURE 3: Comparative far-UV CD spectra of human UCPs in DDM. Far-UV CD spectra of hUCPs in 10 mM potassium phosphate buffer (pH 7.5) containing 0.03% DDM and UCP2 in 10 mM Tris buffer (pH 7.5) containing 0.03% DDM, at 25 °C. The spectra are normalized at 220 nm for comparison. The protein concentrations were 5 μM (hUCP1), 3.8 μM (hUCP2), 2.5 μM (hUCP3), 2.5 μM (hUCP4), and 4.8 μM (hUCP5).

centration was close to the critical micellar concentration (CMC) at 0.59 mM for DDM (CMC = 0.15 mM) (*24*). As seen in Figure 3, the CD spectra of hUCPs 1, 3, and 5 were almost identical with one major negative maximum at ~222 nm and a positive maximum approaching 190 nm, as well as a shoulder at ~208 nm. The CD spectrum of hUCP4 in DDM was different and showed two negative maxima at 208 nm (higher ellipticity) and 222 nm and a positive maximum at ~192 nm. The CD spectrum of hUCP2 in Tris buffer was in between these two groups of spectra, with two negative maxima at 208 nm (lower ellipticity) and 222 nm. This spectrum shows the influence of buffer and ionic strength on the reconstitution and conformation of UCPs in DDM. The overall spectra of the proteins in detergent indicate the presence of both helical and β-structure components. Overall, on the basis of CD deconvolution analyses results, the conformations of all five proteins had some helical content in DDM, with hUCP4 having the highest helical content. The deconvolution of CD spectra for UCPs 4 and 5 revealed 23% and 23% helix, 29% and 23% β-sheet, 21% and 19% β-turn, and 27% and 35% unordered structures, respectively. CD spectra of UCPs 1 and 3 were comparable to those of UCP5. UCP2 spectra in Tris buffer showed less than 10% helical content and was dominantly β-sheet (35%) and nonordered (~40%). These results imply that UCPs may not be fully refolded in DDM. Overall, in comparison with DDM, reconstituted UCPs in digitonin had a higher helical content, and their CD spectra were comparable to those of reconstituted proteins in liposomes, which will be discussed in the next section.

Previous structural analysis of His-tagged and nontagged mouse UCP1 (89% sequence identity to human UCP1) in 0.02% digitonin has shown dominantly helical conformations (*11*). In addition to the differences in primary structure and the degree of purity, stabilization of the protein in detergents may also affect the overall helical content of the protein. The differences in the CD spectra may also be attributed to dissimilar packing of the TM domains in protein monomers and variable degrees of monomer association. It has also been shown that the addition of a His tag does not significantly affect the secondary structure of hUCP1 when reconstituted in detergents (*11*). In the present study, all five UCPs include a His_6 tag and a seven amino acid TEV protease site, and it seems plausible that the overall

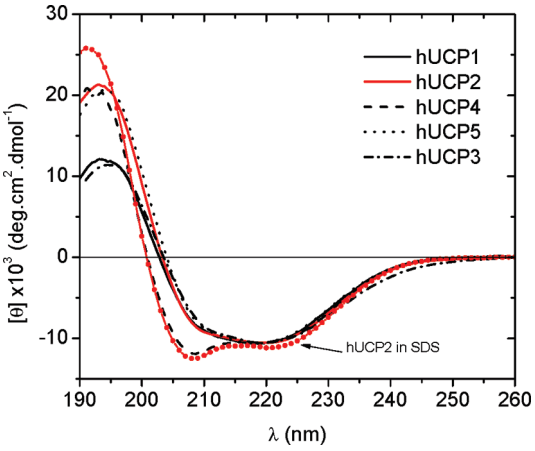

FIGURE 4: Comparative far-UV CD spectra of human UCPs in liposomes. The proteins were reconstituted in 500 μM SUVs (POPC/POPG 7:3 molar ratio) in buffer composed of 10 mM potassium phosphate (pH 7.5) at 25 °C. The spectra are normalized at 220 nm for comparison. The protein concentrations were 5.7 μM (hUCP1), 4.3 μM (hUCP2), 6.8 μM (hUCP3), 5 μM (hUCP4), and 7.4 μM (hUCP5).

conformation of the proteins is not significantly affected by these additions.

Conformation of Neuronal hUCPs Reconstituted in Small Unilamellar Vesicles. The reconstitution system of POPC/POPG (7:3 molar ratio) is a stable bilayer system for SUV formation and roughly represents the negatively charged inner mitochondrial membrane. The normalized far-UV CD spectra of hUCPs, reconstituted in liposomes, can be seen in Figure 4. These spectra reveal dominantly helical profiles for all UCPs. UCPs 1 and 3 seemed to have lower helical contents than expected due to their low positive maximum ellipticities, which could be an artifact due to flattening effects caused by light scattering at wavelengths below 200 nm (*25*). Generally, the CD spectra of UCPs 2 and 5 (as well as UCPs 1 and 3) have a negative maximum at ~220 nm, a shoulder at ~210 nm, and a positive maximum at ~194 nm, with the positive maximum to negative maximum ratio of about 1.5:1 (~1:1 for UCPs 1 and 3). On the other hand, hUCP4 has two dominant negative maxima at 208 and 220 nm with a positive maximum at ~193 nm and a positive maximum to negative maximum ratio of 2:1 (typical for helical structures). Estimates of the secondary structure compositions, normalized on the basis of the hUCP4 CD spectrum at 220 nm (Table 2), suggest that hUCP4 has the highest helical content at 37%, followed by hUCP2 at 34%, hUCPs 3 and 5 at 33%, and hUCP1 at 31%. Among the hUCPs, hUCP4 conformation seems to be unique and different from the conformation of the other hUCPs (Figures 3 and 4 and Table 2).

The calculated helical content as defined by the six TM domains of the primary structure of the proteins on the basis of hydrophobicity scales (and sequence alignment with ANT1) is 40% (55%) for hUCP1, 39% (54%) for hUCPs 2 and 3, 37% (52%) for hUCP4, and 33% (52%) for hUCP5 (Table 2). These calculations and their comparison with experimental results based on CD analysis of protein conformations may indicate that UCPs were not fully folded in liposomes. Interestingly, the CD spectra of UCPs in SDS micelles (in water) and 80% trifluoroethanol exhibited typical α-helical profiles. It is assumed that both SDS and trifluoroethanol can unfold the tertiary and quaternary structure of proteins, while retaining most of their helical structures. The CD spectrum of UCP2 in SDS can be compared to other UCPs in Figure 4. The protein is unfolded, and its overall helical structure is more apparent. The data indicated that SDS stabilizes a substantial part of the protein's helical structure, but the helices are unpacked (less interhelical interaction). UCP2 in SDS and trifluoroethanol is 42−46% helical, 15−18% β-sheet, and ~25% unordered (Table 2). The overall helix content of UCPs in helix-stabilizing environments is therefore in between the calculated values based on hydrophobicity scales and sequence alignment with ANT1. In addition to spectral artifacts due to the flattening effect, the lower helical content in UCPs may be due to association of monomers and/or differential helix packing within monomers (*11*). It has been previously suggested that UCP's functional form is dimeric, where a C-terminal solvent-exposed cysteine residue (Cys^{304}, unique to UCP1) plays a role in disulfide bond formation between UCP1 monomers (*26*).

Table 2: Secondary Structure Composition of Human UCPs in Lipid Vesicles[a]

protein	α-helix	β-strand	turn	random	NRMSD
hUCP1-PC/PG	31	19	20	31	0.013
hUCP2-PC/PG	34	24	19	23	0.011
hUCP3-PC/PG	33	18	18	31	0.024
hUCP4-PC/PG	37	16	19	27	0.011
hUCP5-PC/PG	33	27	21	20	0.010
hUCP2-SDS	42	15	18	25	0.008
hUCP2-TFE	46	18	14	22	0.007

[a]Deconvolution of the CD spectra was performed using the CDSSTR program on the Dichroweb website (see the Experimental Procedures section). The values represent the percentage of secondary structure composition. NRMSD, normalized root mean square deviation, denotes the best fit between the calculated and experimental CD spectra. Spectra were normalized at 220 nm for comparison. Analysis of the hUCP2 spectra in 20 mM SDS and 80% TFE in water is also given. Both SDS and TFE denature the tertiary and quaternary structures but stabilize and promote the secondary structures in proteins.

Furthermore, it is important to note that the available deconvolution methods used for CD spectral analysis can only give estimates of the structural composition of membrane proteins, since the reference data sets used for calculating the secondary structure content are primarily based on known structures of soluble globular proteins. It has been shown that reference databases derived from soluble proteins are less reliable when applied to membrane protein CD spectral analyses (*27*). In membrane proteins, α-helices can be classified into two types: α-helices in soluble domains and TM α-helices. Two main differences between these two helix types contribute to the differences in observed CD spectra: (i) the rotational strength of the TM helix is larger in intensity than that of the soluble helix, which can be attributed to the different dielectric media that the two helices are in, and (ii) the average chain length of the membrane-spanning helices is about 24 residues, which is about twice the average chain length of α-helices of soluble proteins, resulting in different intensities of CD spectra (*28*). Since UCPs are mainly composed of TM helices, they are expected to have different characteristic spectra from a typical soluble helix. In addition, it has been shown that in helices embedded in lipid membranes the stronger $\pi \rightarrow \pi^*$ transition, which governs the intensity of the 192 and 208 nm bands, is expected to be more sensitive to the TM chain length, and the 208 nm band appears to be missing in shorter helices, as seems to be the case with UCPs 1, 2, 3, and 5 (*29*). This assumption, however, does not correlate to UCPs with the relatively long average TM helix lengths. Therefore,

there must be another explanation as to why the 208 nm band is hidden as a shoulder in the spectra of UCPs 1, 2, 3, and 5 but not in the spectra of UCP4 or the UCP2 in SDS micelles. UCPs 1, 2, 3, and 5 are likely to partly self-associate when reconstituted in lipid bilayers, and this is reflected in the lower ellipticities of the bands at ~208 nm (compared to the $n \rightarrow \pi^*$ band at ~220 nm). Moreover, studies using mild detergent systems have shown that UCP1 may be able to form dimers, which could be also the case of UCPs in lipid membrane bilayers (Figures 3 and 4) (*1*). On the other hand, the deviation of the CD spectra of these proteins from typical α-helical spectra can also be the result of close packing of helical TM domains (*11*). Conformational changes of UCPs in SDS micelles, which disrupt the interaction between helices as well as protein monomers, support both the close interaction of TM helices and association of monomers in liposomes. UCP4 exhibits a different CD spectrum profile reminiscent of a typical α-helix conformation (comparable to the conformation of UCPs in SDS), which can be related to its less associated (monomeric) form in proteoliposomes or detergents (Figures 3 and 4). Further evidence for the presence of the associated forms of UCPs 1, 2, and 5 and a mixture of associated and monomeric forms for hUCP4 has been observed in blue-native gel electrophoresis profiles of these proteins in detergents (Tuan Hoang, unpublished results). As previously mentioned, in addition to association of UCP monomers, another possible explanation for the difference in spectral profiles can be due to the differences in the packing and folding of helices and the overall tertiary structure of these proteins. Possible close helix−helix interactions of the coiled-coil type may occur if hydrophobic residues are arrayed along one face of each helix, which is also dependent on the size of the central residues and the helix axis angle (*30*, *31*).

Inhibitor and Activator Binding to Neuronal hUCPs Reconstituted in Small Unilamellar Vesicles. It has been shown that purine di- and triphosphate nucleotides strongly bind to UCP1 and inhibit its ion-transport function (*1*). In order to show that the proteins are in their natively folded and functional form, guanosine di- and triphosphate nucleotides were used to study the structure−function relationship of the neuronal hUCPs. Furthermore, lauric acid (LA) was used to study the activating effect of fatty acids on the reconstituted UCPs. Spectroscopic studies were also performed on the interaction of CoA with UCPs. CoA is in close proximity to the native environment of UCPs in the mitochondria and is involved in lipid transport and metabolism, and it is therefore worthwhile to investigate its possible effect on the structure and function of UCPs.

The nucleotide binding site in UCP1 involves three basic amino acids, Arg^{84}, Arg^{183}, and Arg^{277}, which are conserved in all five members of the mammalian UCP family (Figure 1). In close proximity (±9 residues) to the Arg residues are two conserved Trp residues, Trp^{174} and Trp^{281}. Hence, detection of nucleotide binding can be potentially observed by the changes in the microenvironment of these aromatic amino acids, as well as other Tyr and Trp residues in close proximity to the binding site. Proteins hUCP1, hUCP2, hUCP3, hUCP4, and hUCP5 contain 2, 2, 2, 8, and 6 Trp residues, as well as 8, 11, 12, 10, and 10 Tyr residues, respectively (Table 1).

Purine nucleotides strongly bind to UCP1 to inhibit its ion transport, and this known function has been used to test the correct reconstitution and folding of the native protein into SUVs. The interaction of reconstituted nUCPs with GDP and GTP can be seen in Figure 5A. The far-UV spectra of all three proteins exhibit minor conformational changes upon binding to the purine nucleotides. Only in UCP4 are the changes in the spectra more obvious, with the lowest ellipticity for the CD spectrum of the GDP-bound protein. The near-UV spectra of UCP4 (inset) also have a very different profile from those of UCPs 2 and 5 (insets), with a low intensity and three prominent maxima at approximately at 300, 280, and 260 nm. Upon nucleotide binding in UCP4, the overall near-UV spectra increase in intensity, keeping the three maxima at the same relative positions. Compared with the GTP binding, GDP binding to UCP4 shows a stronger increase in the 280 nm maximum and a decrease in the 300 nm maximum, which can imply that binding of these nucleotides to UCP4 is not occurring in the same manner. The nucleotide binding to UCPs 2 and 5 was comparable and showed slightly different spectra for the two nucleotides. Upon GDP binding, the near-UV CD spectra of UCPs 2 and 5 increased with a slight blue shift of the maximum from ~290 to ~285 nm. In comparison with GDP, binding of GTP to both proteins showed a more prominent shift in the spectrum to 280 nm, with lower intensity for UCP2 and higher intensity for UCP5. Overall, nucleotide-bound proteins were significantly different from free protein in the near-UV region. The far- and near-UV spectra for the free and bound UCPs 1 and 3 exhibited features comparable to those of UCPs 2 and 5 (data not shown) (*11*).

Conformational studies of the interaction of nUCPs with LA and CoA are exhibited in Figure 5B. The far-UV CD spectra of interaction of LA and CoA with UCP2 and UCP5 are almost indistinguishable from those of the free proteins. In UCP4, compared to the spectrum of the free protein, the spectrum for CoA interaction has a lower overall ellipticity, whereas the spectrum of the LA interaction is comparable. Near-UV CD spectra of the analysis can be seen in the insets of Figure 5B. In UCP2, the changes in the spectra are comparable, but in UCP5 the spectra of interactions with LA and CoA are different from each other. As mentioned above, the near-UV spectra of UCP4 are drastically different from those of UCPs 2 and 5, indicative of an overall different microenvironment for aromatics (mainly Trp and Tyr) and tertiary structure of this protein. Interaction of UCP4 with LA shows a 2-fold increase in the intensity at the 280 nm maximum, in comparison with the free protein. The LA and CoA interaction spectra have minor differences, of which a broad maximum for CoA and a sharp maximum at 285 nm for LA were most distinct.

Overall, these results suggest different modes of interaction for LA and CoA with nUCPs. The role that fatty acids play in activating UCPs has been extensively studied and suggested the involvement of acidic residues close to the surface and core of the protein required for fatty acid-mediated proton transport (*2*). Fatty acids have not been shown to directly bind UCPs at a specific site, and hence no plausible explanation involving aromatic amino acids can be derived at present. On the other hand, CoA is notably involved in the synthesis and oxidation of fatty acids, as well as in the import of fatty acids into the mitochondria (*32*). Structurally, CoA has a purine nucleotide moiety on one end, a hydrophobic zone in the middle, and a thiol group on the other end of the molecule. Considering that ADP and ATP are capable of binding to and inhibiting UCPs, it is plausible to suggest that CoA may bind to UCPs through its adenine-containing nucleotide component. This suggestion is supported by the near-UV CD spectra of interaction of CoA with nUCPs,

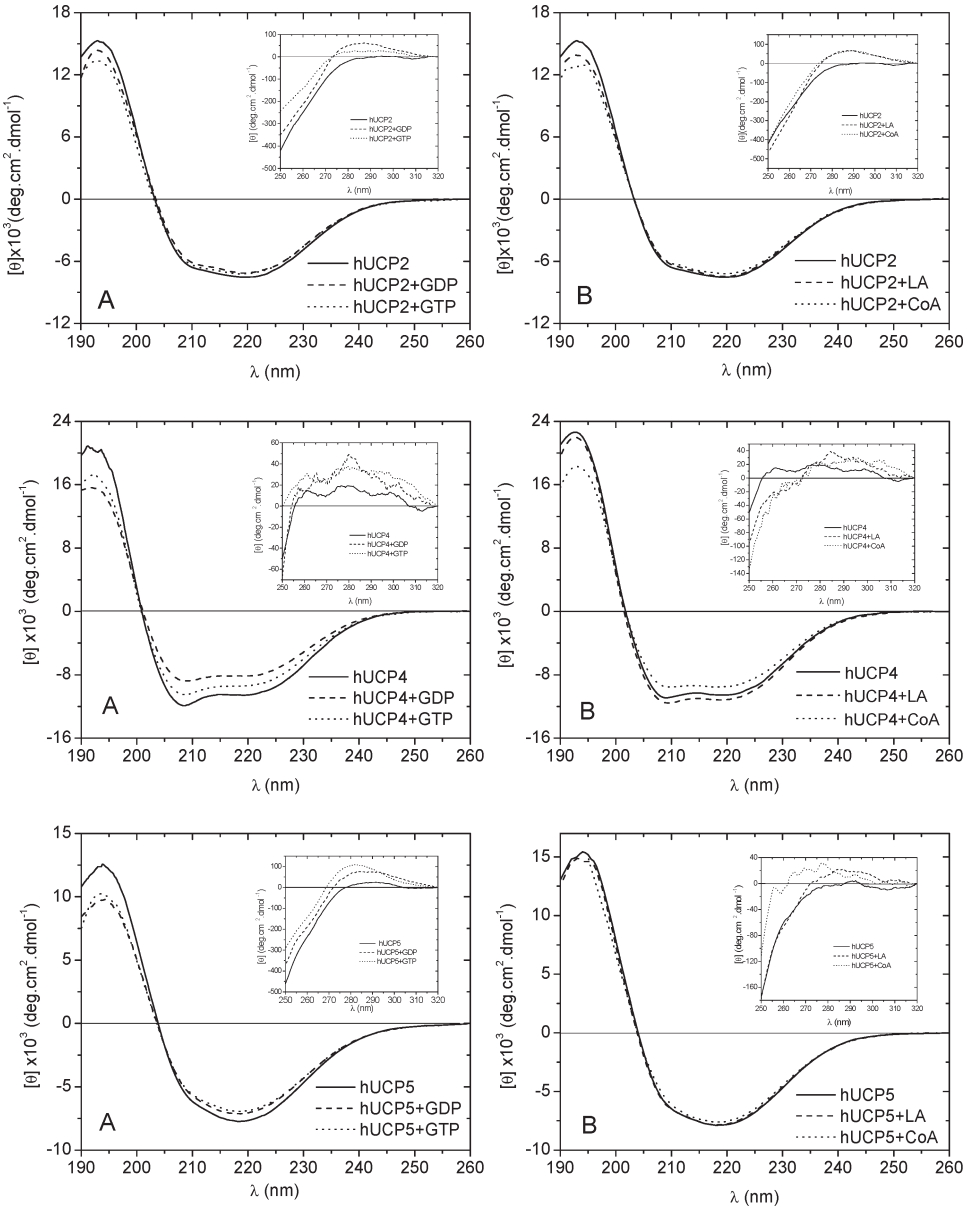

FIGURE 5: CD spectra of neuronal hUCPs in liposomes with purine nucleotide inhibitors, fatty acid activator, and CoA. (A) The far-UV and near-UV (inset) spectra of nUCPs with GDP and GTP inhibitors. (B) The far-UV and near-UV (inset) spectra of nUCPs with LA activator and CoA. The proteins were reconstituted in 500 μM SUVs (POPC/POPG 7:3 molar ratio) in a buffer composed of 10 mM potassium phosphate (pH 7.5) at 25 °C. The protein concentrations were 4.3 μM (hUCP2), 5 μM (hUCP4), and 7.8 and 7.4 μM (hUCP5 in panels A and B, respectively). GTP, GDP, CoA, and LA concentrations were 100 μM.

resembling those of GTP and GDP (Figure 5), and also by the fluorescence spectroscopy data to be discussed in the next section.

Ligand Binding of Neuronal hUCPs As Detected by Fluorescence Spectroscopy. The intrinsic fluorescence studies of nUCPs were made possible by the presence of Trp and Tyr residues found in the vicinity of the nucleotide binding site. The two conserved Trp residues (near TM4 and TM6) in all UCPs (Figure 1) are most useful for studying the purine nucleotide binding, as they form a comparable basis for the four proteins and their interaction with GDP and GTP. The fluorescence spectra of UCP1 with and without GDP/GTP (data not shown) suggest that upon binding of GDP or GTP the microenvironments of the aromatic amino acids are significantly changed, as observed in the 1.5-fold decrease in fluorescence. This decrease in intensity could be indicative of quenching of the fluorescence of aromatic residues. The binding of a ligand to a protein may directly affect the fluorescence of a Trp/Tyr residue by acting as a quencher (by a collisional or energy transfer mechanism) or by physically interacting with the intrinsic fluorophore and thereby changing its overall microenvironment (*33*). Of all aromatic amino acids, Trp is the most sensitive intrinsic fluorophore to environmental changes and also has the highest molar extinction coefficient (ε_{max}). The maximum emission wavelength $\lambda_{max(em)}$ at ~350 nm generally indicates that the Trp residues are more exposed to a polar environment; meanwhile, $\lambda_{max(em)}$ at wavelengths below 350 nm suggests a less polar and more hydrophobic environment for Trp residues. In order to minimize the effect of other aromatic amino acids on the emission spectra of Trp residues in UCPs, the proteins were excited at 295 nm (λ_{ex} 295 nm), where the absorption of Phe and Tyr residues and, hence, their emission are minimal.

Fluorescence spectra (λ_{ex} 295 nm) of the interaction of purine nucleotides LA and CoA with nUCPs are exhibited in Figure 6. Nonbinding purine monophosphate nucleotides, such as AMP,

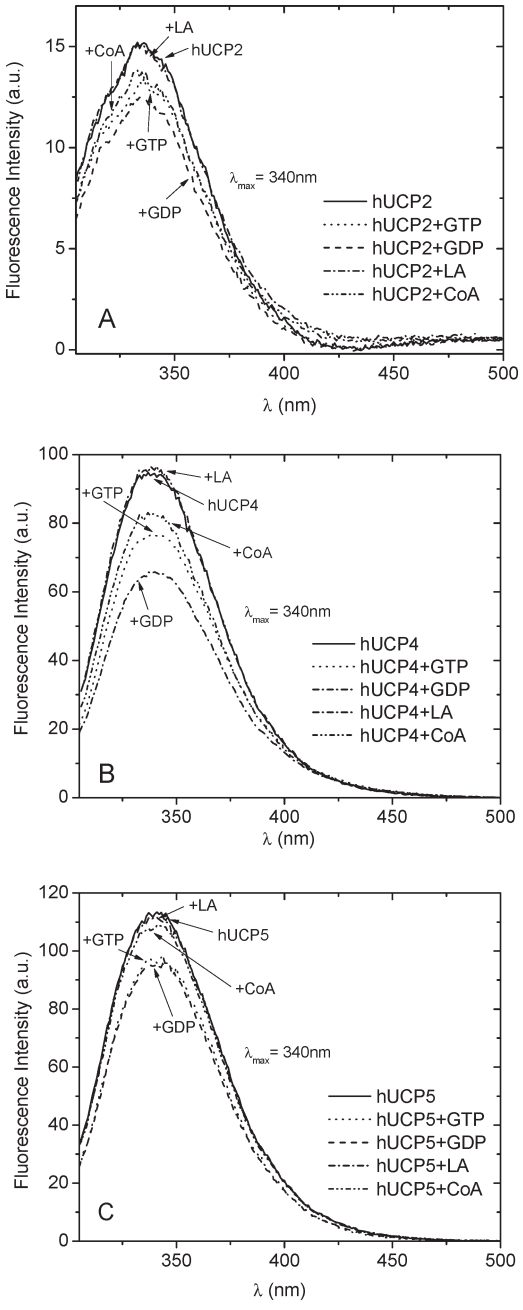

FIGURE 6: Fluorescence spectra of neuronal hUCPs in liposomes with purine nucleotide inhibitors, fatty acid activator, and CoA. Emission spectra of (A) hUCP2, (B) hUCP4, and (C) hUCP5 with GDP, GTP, LA, and CoA. The protein was reconstituted in 500 μM SUVs (POPC/POPG 7:3 molar ratio) in a buffer composed of 10 mM potassium phosphate (pH 7.5) at 25 °C. The protein concentrations were 4.3 μM (hUCP2), 5 μM (hUCP4), and 7.4 μM (hUCP5). GTP, GDP, CoA, and LA concentrations were 100 μM. The excitation wavelength was at 295 nm.

were employed as a negative control to indicate the lack of ligand binding to UCPs. Under our experimental conditions, upon addition of AMP to UCP proteoliposomes, no change in the fluorescence spectra was observed. As seen in Figure 6A, in comparison to the hUCP2 (two Trp residues) spectrum, the emission spectra for the interacting purine nucleotides and CoA were reduced, but the spectrum for LA addition remained unchanged. Interaction of UCP2 with GDP had the lowest emission (Figure 6A). The same trend can be observed for the emission spectra of hUCP4 (eight Trp residues) and hUCP5 (six Trp residues), as exhibited in Figure 6B,C, respectively. As was the case with UCPs 1 and 3 (data not shown), the overall $\lambda_{max(em)}$ (~340 nm) for the spectra of nUCPs did not change in the presence of nucleotides, indicating an overall less polar and more hydrophobic environment of the Trp residues. In the presence of LA, the overall spectra in all nUCPs remained unchanged, suggesting that the aromatic amino acids resided in the same overall environment and/or that binding to LA was not occurring. Upon the addition of CoA, however, the spectra lost their original intensity but were still more intense than the emission of proteins with added GDP and GTP.

Details of the interaction of CoA with hUCPs is not clear; however, as suggested previously, it may have a similar binding site as purine nucleotides due to the presence of the nucleotide phosphate group (with three phosphates) in the molecule. This hypothesis can be further supported by the fact that the spectra of GDP/GTP addition and CoA addition show similar changes from the free protein spectra.

The fluorescence spectra of proteins in lipid vesicles, shown in Figure 6, further support the near-UV CD data of the interactions between nUCPs with purine nucleotides LA and CoA. Put together, the studies suggest that upon binding to nucleotides all three proteins undergo a minor conformational change that changes the microenvironment of the aromatic amino acids close to the nucleotide binding site; the same changes occur when the λ_{ex} is at 280 nm, which results in the cumulative emission of both Trp and Tyr residues (data not shown). Similarly, CoA addition causes a modification in the environment of specific aromatic amino acids, suggesting a possible interaction between the molecule and UCPs, most likely at the nucleotide binding site. Interestingly, for LA interaction the near-UV CD spectra suggest a definite microenvironment change of certain aromatic amino acids in all nUCPs; however, the fluorescence data showed no significant changes in the fluorescence of the aromatic residues. This observation still implies that LA may interact with and nonspecifically bind to the protein surface. Furthermore, at neutral pH, LA (or any other fatty acid) is negatively charged and is therefore unable to freely flip across the bilayer membrane and interact with the UCPs on the inner phospholipid monolayer leaflet or in the hydrophobic membrane core, but it can still interact with the protein and phospholipids on the outer monolayer leaflet, causing minor conformational changes in the tertiary structure of UCPs.

CONCLUSION

In this study it has been shown that hUCPs were dominantly helical in phospholipid SUVs modeling the inner membrane of mitochondria. As observed in the far- and near-UV CD spectra, of all neuronal hUCPs, hUCP4 had a conformation distinct from the rest of the hUCPs and was the most helical. It has been suggested that while hUCP4 can retain part of its monomeric features in membrane-like environments, other hUCPs tend to associate and possibly form dimers. In addition to the detailed comparative CD conformational analysis of neuronal UCPs, another feature of this study is the reconstitution of functional or partially functional folded forms of neuronal hUCPs in SUVs. Nucleotide binding is known to occur from the intermembrane side of UCPs, whereas fatty acid binding is hypothesized to be from the matrix side. The functional topology/orientation of the reconstituted hUCPs is supported by (i) the observed nucleotide binding to hUCPs 1−5 as detected by the near-UV CD and

fluorescence spectra, implying the existence of functional proteins with both C- and N-termini located at the outer surface of the liposome, and (ii) the lack of specific binding of LA to the proteins as observed in the unchanged fluorescence spectra. Overall, despite dissimilar primary sequences, UCPs share common structural and functional properties. This finding is especially important for the less studied UCPs 4 and 5, with relatively low sequence identity with UCPs 1−3, emphasizing their primary roles as uncoupling proteins. On the basis of the results of this study, we have initiated more detailed comparative biophysical investigations in our laboratory to further clarify the diversity of the biochemical and physiological roles of the uncoupling proteins.

REFERENCES

1. Echtay, K. S. (2007) Mitochondrial uncoupling proteins—what is their physiological role? *Free Radical Biol. Med. 43*, 1351–1371.
2. Krauss, S., Zhang, C. Y., and Lowell, B. B. (2005) The mitochondrial uncoupling protein homologues. *Nat. Rev. Mol. Cell Biol. 6*, 248–261.
3. Fleury, C., Neverova, M., Collins, S., Raimbault, S., Champigny, O., Levi-Meyrueis, C., Bouillaud, F., Selding, M. F., Surwit, R. S., Ricquier, D., and Warden, C. H. (1997) Uncoupling protein-2: a novel gene linked to obesity and hyperinsulinemia. *Nat. Rev. Genet. 15*, 269–272.
4. Mao, W., Yu, X. X., Zhong, A., Li, W., Brush, J., Sherwood, S. W., Adams, S. H., and Pan, G. (1999) UCP4, a novel brain-specific mitochondrial protein that reduces membrane potential in mammalian cells. *FEBS Lett. 443*, 326–330.
5. Sanchis, D., Fleury, C., Chomiki, N., Goubern, M., Huang, Q., Neverova, M., Grégoire, F., Easlick, J., Raimbault, S., Lévi-Meyrueis, C., Miroux, B., Collins, S., Seldin, M., Richard, D., Warden, C., Bouillaud, F., and Ricquier, D. (1998) BMCP1, a novel mitochondrial carrier with high expression in the central nervous system of humans and rodents, and respiration uncoupling activity in recombinant yeast. *J. Biol. Chem. 273*, 34611–34615.
6. Andrews, Z. B., Diano, S., and Horvath, T. L. (2005) Mitochondrial uncoupling proteins in the CNS: in support of function and survival. *Nat. Rev. Neurosci. 6*, 829–840.
7. Chan, S. L., Liu, D., Kyriazis, G. A., Bagsiyao, P., Ouyang, X., and Mattson, M. P. (2006) Mitochondrial uncoupling protein-4 regulates calcium homeostasis and sensitivity to store depletion-induced apoptosis in neuronal cells. *J. Biol. Chem. 281*, 37391–37403.
8. Andrews, Z. B., Liu, Z.-W., Walllingford, N., Erion, D. M., Borok, E., Friedman, J. M., Tschop, M. H., Shanabrough, M., Cline, G., Shulman, G., Coppola, A., Gao, X.-B., Horvath, T. L., and Diano, S. (2008) UCP2 mediates ghrelin's action on NPY/AgRP neurons by lowering free radicals. *Nature 454*, 846–851.
9. Conti, B., Sugama, S., Lucero, J., Winsky-Sommerer, R., Wirz, S. A., Maher, P., Andrews, Z., Barr, A. M., Morale, M., Paneda, C., Pemberton, J., Gaidarova, S., Behrens, M. M., Beal, F., Sanna, P. P., Horvath, T. L., and Bartfai, T. (2005) Uncoupling protein 2 protects dopaminergic neurons from acute1,2,3,6-methyl-phenyl-tetrahydropyridine toxicity. *J. Neurochem. 93*, 493–501.
10. Echtay, K. S., Winkler, E., Bienengraeber, M., and Klingenberg, M. (2000) Site-directed mutagenesis identifies residues in uncoupling protein (UCP1) involved in three different functions. *Biochemistry 39*, 3311–3317.
11. Jelokhani-Niaraki, M., Ivanova, M. V., McIntyre, B. L., Newman, C. L., McSorley, F. R., Young, E. K., and Smith, M. D. (2008) A CD study of uncoupling protein-1 and its transmembrane and matrix-loop domains. *Biochem. J. 411*, 593–603.
12. Klingenberg, M., and Huang, S. G. (1999) Structure and function of the uncoupling protein from brown adipose tissue. *Biochim. Biophys. Acta 1415*, 271–296.
13. Keller, P. A., Lehr, L., Giacobino, J.-P., Charnay, Y., Assimacopoulos-Jeannet, F., and Giovannini, N. (2005) Cloning, ontogenesis, and localization of an atypical uncoupling protein 4 in *Xenopus laevis*. *Physiol. Genomics 22*, 339–345.
14. Hanák, P., and Ježek, P. (2001) Mitochondrial uncoupling proteins and phylogenesis—UCP4 as the ancestral uncoupling protein. *FEBS Lett. 495*, 137–141.
15. Echtay, K. S., Liu, Q., Caskey, T., Winkler, E., Frischmuth, K., Bienengreber, M., and Klingenberg, M. (1999) Regulation of UCP3 by nucleotides is different from regulation of UCP1. *FEBS Lett. 450*, 8–12.
16. Compton, L. A., and Johnson, W. C. (1986) Analysis of protein circular dichroism spectra for secondary structure using a simple matrix multiplication. *Anal. Biochem. 155*, 155–167.
17. Johnson, W. C. (1999) Analyzing protein circular dichroism spectra for accurate secondary structures. *Proteins: Struct., Funct., Genet. 35*, 307–312.
18. Whitmore, L., and Wallace, B. A. (2004) DICHROWEB: an online server for protein secondary structure analyses from circular dichroism spectroscopic data. *Nucleic Acids Res. 32*, W668–673.
19. Lees, J. G., Miles, A. J., Wien, F., and Wallace, B. A. (2006) A reference database for circular dichroism spectroscopy covering fold and secondary structure space. *Bioinformatics 22*, 1955–1962.
20. Douette, P., Navet, R., Bouillenne, F., Brans, A., Sluse-Goffart, C., Matagne, A., and Sluse, F. E. (2004) Secondary-structure characterization by far-UV CD of highly purified uncoupling protein 1 expressed in yeast. *Biochem. J. 380*, 139–145.
21. Rial, E., Muga, A., Valpuesta, J. M., Arrondo, J.-L.R., and Goni, F. M. (1990) Infrared spectroscopic studies of detergent-solubilized uncoupling protein from brown-adipose-tissue mitochondria. *Eur. J. Biochem. 188*, 83–89.
22. Pebay-Peyroula, E., Dahout-Gonzalez, C., Kahn, R., Trézéguet, V., Lauquin, G.J.-M., and Brandolin, G. (2003) Structure of mitochondrial ADP/ATP carrier in complex with carboxyatractyloside. *Nature 426*, 39–44.
23. Skulachev, V. P. (1999) Anion carriers in fatty acid-mediated physiological uncoupling. *J. Bioenerg. Biomembr. 31*, 431–445.
24. O'Neil, M. J. (2006) The Merck Index, 14th ed., Merck & Co., Whitehouse Station, NJ.
25. Mao, D., and Wallace, B. A. (1984) Differential light scattering and absorption flattening optical effects are minimal in the circular dichroism spectra of small unilamellar vesicles. *Biochemistry 23*, 2667–2673.
26. Klingenberg, M., and Appel, M. (1989) The uncoupling protein dimer can form a disulfide cross-link between the mobile C-terminal SH groups. *Eur. J. Biochem. 180*, 123–131.
27. Wallace, B. A., Lees, J. G., Orry, A. J. W., Lobley, A., and Janes, R. W. (2003) Analyses of circular dichroism spectra of membrane proteins. *Protein Sci. 12*, 875–884.
28. Park, K., Perczel, A., and Fasman, G. D. (1992) Differentiation between transmembrane helices and peripheral helices by the deconvolution of circular dichroism spectra of membrane proteins. *Protein Sci. 1*, 1032–1049.
29. Fasman, G. D., Ed. (1996) Circular dichroism and the conformational analysis of biomolecules, Chapters 2−4, Plenum Press, New York.
30. Fasman, G. D., Ed. (1989) Prediction of protein structure and the principles of protein conformation, Chapters 11 and 18, Plenum Press, New York.
31. Taira, J., Jelokhani-Niaraki, M., Osada, S., Kato, F., and Kodama, H. (2008) Ion-channel formation assisted by electrostatic interhelical interactions in covalently dimerized amphiphilic helical peptides. *Biochemistry 47*, 3705–3714.
32. Voet, D., and Voet, J. G. (2004) Biochemistry: biomolecules, mechanisms of enzyme action and metabolism, 2nd ed., Vol. *1*, Chapters 1, 4, 16, 17, and 22, John Wiley and Sons, New York.
33. Eftink, M. R. (1997) Fluorescence methods for studying equilibrium macromolecule-ligand interactions. *Methods Enzymol. 278*, 221–257.
34. Chenna, R., Sugawara, H., Koike, T., Lopez, R., Gibson, T. J., Higgins, D. G., and Thompson, J. D. (2003) Multiple sequence alignment with the clustal series of programs. *Nucleic Acids Res. 31*, 3497–500.